Low- and high-field transport properties of pseudomorphic $In_xGa_{1-x}As/InP$ ($0.73 \leqslant x \leqslant 0.82$) *p*-type modulation-doped single-quantum-well structures

A. Mesquida Küsters, A. Kohl, and K. Heime
Institut für Halbleitertechnik, Lehrstuhl I, RWTH Aachen, D-52056 Aachen, Germany

Th. Schäpers, D. Uhlisch, B. Lengeler, and H. Lüth
Institut für Schicht- und Ionentechnik, Forschungszentrum Jülich, Jülich, Germany

(Received 7 September 1993; accepted for publication 3 December 1993)

The transport properties of three *p*-type modulation-doped $In_xGa_{1-x}As/InP$ ($0.73 < x < 0.82$) single-quantum-well structures grown by metalorganic chemical-vapor deposition are reported. High carrier mobilities of $\mu_H = 7800\ cm^2/V\,s$ coupled with total carrier concentrations of $p_S = 2.1 \times 10^{12}\ cm^{-2}$ were reached, for example, for $x = 0.73$ at 5 K. Shubnikov–de Haas and quantum Hall-effect measurements at 50 mK showed the population of two spin-split $V_{3/2}$ subbands. Using *p*-modulation-doped field-effect transistors with a gate length of $L_G = 1\ \mu m$, fabricated on the same samples, the carrier transport at moderate and high fields was investigated at 77 K. Thereby, the population of the heavy-hole subband and, above a critical field, also the occupation of the light-hole subband were verified. With the help of dc transconductance (g_{mext}-V_{GS}) and magnetotransconductance measurements a decoupling between both subbands at cryogenic conditions and moderate fields was observed, resulting in two clearly defined conducting channels. Further analysis of the measured mobility-voltage (μ-V_{GS}) and velocity-field (v_{avg}-E_{avg}) profiles revealed that carrier transport in compressively strained two-dimensional hole gas (2DHG) systems is strongly affected by intersubband scattering and shows a nonlinear behavior at low fields, caused by the zone-center degeneracy of their E-$k_{\|}$ distribution.

I. INTRODUCTION

Pseudomorphic $In_xGa_{1-x}As/InP$ *p*-channel field-effect transistors (FETs) show a high potential for low-power complementary microwave integrated circuits because of their improved performance based on the better transport characteristics of In-rich $In_xGa_{1-x}As$ channels.[1–3] Theoretical calculations and experimental results indicate that the introduction of compressive strain in an $In_xGa_{1-x}As$ quantum well (QW) on InP—i.e., increased In mole fraction—lifts the zone-center degeneracy of the so-called "heavy-hole" ($HH, V_{3/2}, |3/2, \pm 3/2\rangle$) and "light-hole" ($LH, V_{1/2}, |3/2, \pm 1/2\rangle$) bands and results in a reduction of the in-plane hole effective mass.[4–6] On the other hand, the effective mass in the growth direction increases, resulting in a better confinement of the carriers in the QW. The valence-band discontinuity ΔE_V between $In_xGa_{1-x}As$ and InP is high and lies for the investigated samples, between $\Delta E_V = 0.42$ for $x = 73\%$ and $\Delta E_V = 0.48$ for $x = 82\%$,[6] guaranteeing a good confinement of the carriers in the channel. A modulation-doped design results in higher mobilities for the holes in the QW due to the reduction of Coulomb scattering, and the double heterojunction approach provides high carrier densities at the same time. In the following sections we describe the transport characteristics of three optimized pseudomorphic samples with indium mole fractions of 73%, 77%, and 82% employing temperature-dependent Shubnikov–de Haas, quantum Hall-effect, and van der Pauw measurements for low-field conditions and dc I_{DS}/V_{GS} and magnetotransconductance measurements for moderate- and high-field conditions.

II. EXPERIMENT

Figure 1 shows the cross section of the optimized *p*-type modulation-doped QW heterostructures. In our structure the strained $In_xGa_{1-x}As$ channel is sandwiched between two undoped InP spacers and two *p*-doped InP carrier supplying layers. These five layers were carefully optimized depending on strain and channel thickness. An extended report about the optimization procedure of these structures can be found in Refs. 1 and 7. The 330-nm-thick *u*-InP buffer layer and the p^{++}-InGaAs contact layer are less critical for the performance of the structures. Our objective was the achievement of the highest possible carrier concentration in the channel without parallel conduction in the lower *p*-InP doping layer. A strong dependence of the carrier transfer into the channel on the strain level in the $In_xGa_{1-x}As$ QW was experimentally measured with the help of various characterization methods.[1,7] The observed enhancement of the hole concentration with increasing strain can be explained by the stronger influence of the QW on the carrier transfer due to the higher-valence-band discontinuity ΔE_V. The improvement of biaxial stress results in a higher population of the degenerated $V_{3/2}$ band in the channel and reduces the overall hole effective mass near the Γ point.[2,3] With the help of five samples with a QW thickness of 10 nm, strain levels of $x = 64\%$ and 73% and different lower doping layer thicknesses ($10\ nm < d_{dopl} < 50\ nm$, $N_{A2} = 8 \times 10^{17}\ cm^{-3}$) we characterized experimentally the dependence of the depleted thickness on strain.[1,7] Using an *a priori* prediction model for higher In mole fractions we found optimum

 0021-8979/94/75(7)/3507/9/$6.00

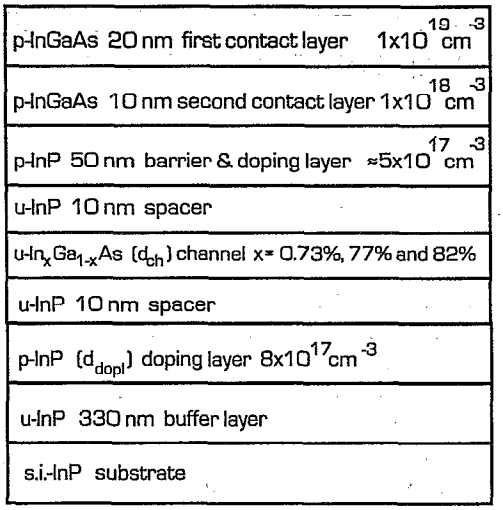

FIG. 1. Cross section of the investigated pseudomorphic $In_xGa_{1-x}As/InP$ p-type modulation doped single-quantum-well heterostructures.

thicknesses of $d_{opt(10\ nm)}=22$, 27, and 34 nm for $x=0.73$, 0.77, and 0.82, respectively, on the assumption that a 10-nm-thick QW is also utilized.[7]

It is well known that the biaxial stress in strained layers can only be retained if the thickness of these layers does not exceed a critical value. For the choice of the channel thickness d_{ch} we used the more conservative prediction of the Matthews and Blakeslee mechanical equilibrium model in accordance with the results of Temkin *et al.*[8] The selected values for $x=0.73$, 0.77, and 0.82 were $d_{ch}=8$, 6, and 4 nm, respectively.

Finally, we calculated the thickness of the lower doping layer d_{dopl} for the selected d_{ch} values, 18, 16, and 12 nm for $x=0.73$, 0.77, and 0.82, respectively.[7] The nonlinear dependence of the quantization effect on the QW thickness reduces the probability of hole transfer from the doping layers if d_{ch} is lowered. This fact results in some inaccuracy concerning the optimum value of d_{dopl}. Nevertheless, only for the sample with $x=77\%$ was a thin bypass channel under the QW observed experimentally (see following sections) indicating the validity of our *a priori* design model.

The samples were grown on (100) semi-insulating InP:Fe substrates by low-pressure metal-organic vapor-phase epitaxy (LP MOVPE). The growth temperature and the total reactor pressure were 640 °C and 20 mbar, respectively. First, an undoped InP buffer layer was grown in order to stop the out-diffusion of impurities from the substrate. After that the lower doping layer with the appropriate thickness d_{dopl} for each structure and a doping concentration of $N_{A2}=8\times10^{17}$ cm^{-3} was deposited, followed by a growth interruption in order to activate electrically the Zn atoms.[9] A 10-nm-thick u-InP spacer and the strained u-$In_xGa_{1-x}As$ channel (d_{ch}) were grown subsequently. The change of growth rate for the strained material was taken into account. On top of the channel a 28-nm-thick u-InP layer followed by a 32-nm-thick p-InP layer ($N_A=5\times10^{17}$ cm^{-3}) were grown. The Zn diffusion during the epitaxy was also considered.[10] For the given growth parameters we calculated an unintentional diffusion of about 18 nm, so that an undoped spacer of about 10 nm thickness remained between the channel and the upper doping layer. Due to the unintentional diffusion the profile of the doping concentration in the upper carrier supplying layer is not constant, showing a maximum near the surface ($N_{A1}\leq5\times10^{17}$ cm^{-3}). Finally, two p^+-InGaAs contact layers with doping concentrations of $N_A=1\times10^{18}$ and 1×10^{19} cm^{-3} and thicknesses of 10 and 20 nm, respectively, were grown to achieve good ohmic contacts. The graded doping technique for the cap layers reduces the access resistance between ohmic metal and channel due to the graded band bending.

All different types of devices utilized for the transport measurements were fabricated using the same technological process based on optical lithography and liftoff techniques. For mesa etching a $HCl:CH_3COOH:H_2O_2$ 6:4:1 solution at 8 °C was employed. Ni:AuZn:Ni was evaporated for the ohmic contacts, followed by 45 s annealing at 415 °C. The contact resistivity r_c, evaluated from transmission line method (TLM) patterns, was very low ($r_c\approx1.5$ Ω mm). Van der Pauw measurements on samples with a cloverleaf geometry were used to determine the Hall mobility and sheet carrier concentration as a function of temperature. Shubnikov–de Haas measurements R_{xx} (SdH) and quantum Hall measurements R_{xy} (QHE) were performed on photolithographically defined Hall bars. For both patterns the top p^+-InGaAs layers were removed employing the selective etchant $H_3PO_4:H_2O_2:H_2O$ (1:1:40) at 20 °C. 1.0-μm-long Ti/Pt/Au gates were defined by liftoff after a channel recess step for the transistors. The ideality factor n of the gate diodes varied from 1.7 to 2.1. The reverse bias behavior of the gate diodes was excellent. Gate-source breakdown voltages V_{GSB} larger than 10 V were measured for all devices. Typical leakage currents were $I_{GS}<100$ nA for a 3 V reverse bias and a diode area of 1×100 μm^2. As a last step Cr/Au was evaporated for interconnection metal.

A He-3 system was used to determine the Shubnikov–de Haas oscillations for various temperatures (0.3–10 K), while the high-field measurements up to 16 T were carried out in a dilution refrigerator at a temperature of 50 mK. During all measurements the samples were kept in the dark.

III. RESULTS AND DISCUSSION

A. Low-field transport measurements

Figures 2(a) and 2(b) show the temperature dependence of the mobility μ_H and sheet hole concentration p_S of the three samples under study, respectively. The results obtained at 5 and 300 K are summarized in Table I. At room temperature the mobility increases from 380 cm^2/V s for the sample with $x=0.73$ up to 400 cm^2/V s for $x=0.82$. While the temperature decreases the mobility of the 2DHG increases substantially due to the decrease of the polar optical-phonon scattering. For the samples with

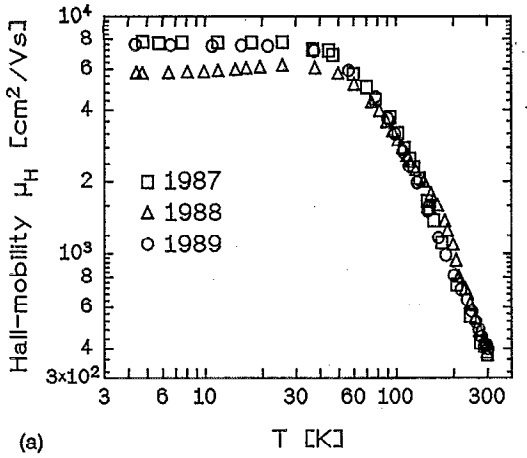

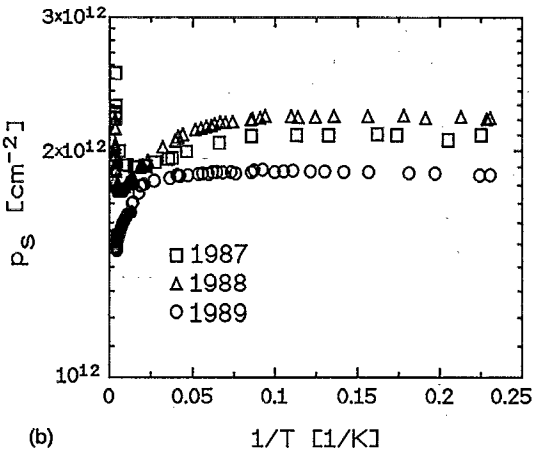

FIG. 2. (a) Measured Hall mobilities μ_H and (b) sheet carrier concentrations p_S of the samples 1987 (x=73%, squares), 1988 (x=77%, triangles) and 1989 (x=82%, circles) between 5 and 300 K.

x=0.73 and 0.82 the mobility is essentially flat below 30 K with values as high as 7800 and 7620 cm^2/V s at 5 K, respectively. Since the hole transport takes place in a ternary material, the mobility is mainly limited by the alloy scattering, which is independent of temperature for degenerate two-dimensional systems. The sample with an intermediate In content (x=0.77) shows a slight decrease of

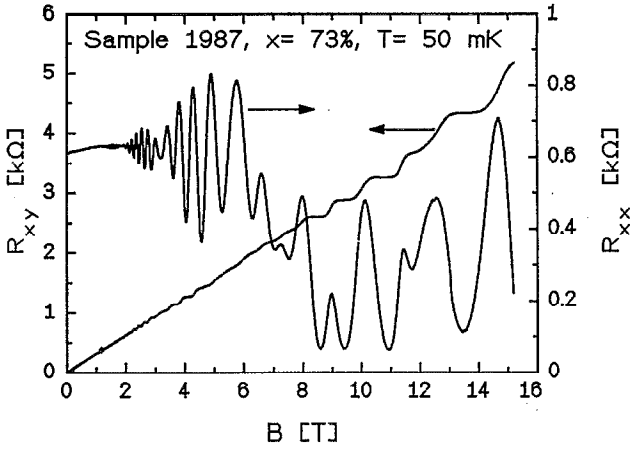

FIG. 3. Measured Shubnikov–de Haas oscillations R_{xy} and quantum Hall effect R_{xx} vs magnetic field of the sample 1987 (x=73%) at 50 mK.

the mobility for temperatures below 30 K. At 5 K a mobility of 5810 cm^2/V s was obtained, which is considerably lower than the values of the samples discussed before. A possible explanation for the observed drop of the mobility by decreasing the temperature is a bypass channel in the lower InP doping layer. This parallel conduction can be observed in Fig. 2(a), where the mobility curve of this sample shows a small shoulder between 140 and 220 K, indicating thermal generation of carriers in the barrier material.

Below 10 K the sheet hole concentration was almost insensitive to the temperature for all three samples as expected for a degenerate two-dimensional hole system. If the temperature was increased from 10 up to 300 K, p_S ran through a local minimum [see Fig. 2(b)]. This can be explained by thermal generation of a small amount of carriers in the InP layers.

In order to gain precise information of the occupation of different subbands in the channel Shubnikov–de Haas (R_{xx}) and quantum Hall-effect (R_{xy}) measurements were performed. Figure 3 shows a plot of R_{xx} and R_{xy} as a function of the magnetic field for the sample 1987 (x =0.73) at 50 mK. Clearly resolved steps of the quantum

TABLE I. Hole mobility μ_H and sheet carrier concentration p_S from Hall measurements at 300 and 5 K as well as total ($p_{S\,\mathrm{QUE}}$) concentration and its distribution ($p_{3/2,1}$,$p_{S3/2,2}$,$p_{1/2}$) extracted from QHE and SdH measurements at 50 mK, respectively, of the three investigated samples.

Sample	1987	1988	1989
In mole fraction x	0.73	0.77	0.82
d_{ch} (nm)	8	6	4
μ_H 300 K (cm^2/V s)	380	390	400
p_S 300 K (cm^{-2})	2.45×10^{12}	2.6×10^{12}	1.92×10^{12}
μ_H 5 K (cm^2/V s)	7800	5810	7620
p_S 5 K (cm^{-2}) 9	2.1×10^{12}	2.2×10^{12}	1.85×10^{12}
p_{QHE} 50 mK (cm^{-2})	2.03×10^{12}	2.07×10^{12}	1.87×10^{12}
$p_{3/2,1}$ 50 mK (cm^{-2})	0.77×10^{12}	0.99×10^{12}	0.80×10^{12}
$p_{3/2,2}$ 50 mK (cm^{-2})	0.87×10^{12}	1.15×10^{12}	0.96×10^{12}
$p_{1/2}$ 50 mK (cm^{-2})	0.39×10^{12}	...	...
$m^*_{3/2}$ ($\times m_0$)	0.14±0.03	0.12±0.03	0.14±0.03

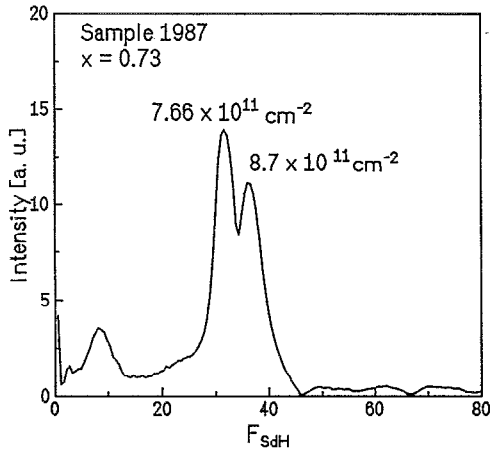

FIG. 4. Calculated Fourier spectrum vs Shubnikov–de Haas oscillation frequency F_{SdH} of the same measurement as in Fig. 3 ($p_{S1\ SdH} = 7.66 \times 10^{11}\,cm^{-2}$, $p_{S2\ SdH} = 8.7 \times 10^{11}\,cm^{-2}$).

Hall effect were detected down to a field of 2 T. Due to the large hole concentration in the channel a minimum filling factor of $i=6$ at a magnetic field of 13 T was observed for this sample. The magnetoresistance R_{xx} was almost constant at low magnetic fields, indicating that no conducting bypass in the Zn-doped InP layers contributed to the carrier transport.

In Fig. 3 the Shubnikov–de Haas oscillations show a characteristic beating effect with nodes at 1.3, 1.83, and 3.2 T. A similar effect was also observed for the samples with $x=0.77$ and 0.82. The beating effect in the Shubnikov–de Haas oscillations originates from a superposition of two oscillations with frequencies close to each other. In order to separate both frequencies a fast Fourier transformation was performed. Since the Shubnikov–de Haas oscillations are periodic in $1/B$, the transformation was calculated relative to $1/B$. The resulting spectrum is shown in Fig. 4. A clear double peak can be observed, which represents two adjacent frequencies leading to the beating effect. The hole concentration p_S of a subband can be deduced from the frequency F_{SdH} of the Shubnikov–de Haas oscillations using the following relation:

$$p_s = s\frac{e}{h}F_{SdH}, \tag{1}$$

where s is the spin degeneracy factor. s can be either 1 for a spin-split or 2 for a spin-degenerate subband. Since a total hole concentration of $p_{QHE}=2.03\times10^{12}\ cm^{-2}$ was deduced from the slope of R_{xy}, the maxima of the double peak must be related to two spin-split subbands belonging to the $V_{3/2}$ valence band. For $s=1$ the position of the peak maxima leads to carrier concentrations of $p_{3/2,1}=7.6\times10^{11}$ cm^{-2} and $p_{3/2,2}=8.77\times10^{11}\ cm^{-2}$ for the spin-down and spin-up $V_{3/2}$ subbands, respectively. If spin-degenerate subbands with $s=2$ are assumed, the sum of $p_{3/2,1}$ and $p_{3/2,2}$ exceed significantly the total carrier concentration p_{QHE} by a value of $0.39\times10^{12}\ cm^{-2}$. Since no conducting bypass was observed in the low-field Shubnikov–de Haas measurement, the difference between $p_{3/2,1}+p_{3/2,2}$ and p_{QHE} must be attributed to the occupation of an additional subband. In the following sections we will demonstrate with other measurement methods that this additional subband is partially occupied (improving its population for higher temperatures and fields) and pertains to the $V_{1/2}$ valence band. For the samples with $x=0.77$ and 0.82 no occupation of this subband at 50 mK was observed. This behavior can be explained by the stronger quantization effect in the last two samples because of their reduced QW thicknesses (see Table I).

The observed spin splitting of the $V_{3/2}$ subbands originates from the lack of inversion symmetry due to an internal electric field perpendicular to the plane of the two-dimensional hole gas. This electric field results in a lifting of the spin degeneracy, which is caused by the spin-orbit coupling.[11,12] A spin splitting of hole subbands was observed before in the material systems InGaAs/InP (Ref. 13) and AlGaAs/GaAs.[14] In the first one, the internal electric field confining the holes to the interface was relatively strong, leading to a large difference in the subband occupation. The ratio $p_{+3/2}/p_{-3/2}$ between the occupation of both subbands was larger than 2. No significant spin splitting was observed for a symmetric AlGaAs/GaAs quantum well, because of a vanishing electric field perpendicular to the interfaces.[14] Since our samples also have a quantum-well geometry, the difference in the carrier density of both spin-split subbands is small. Therefore, the measured ratio $p_{3/2,2}/p_{3/2,1}$ in our samples is also close to one. For $x=0.73$ a ratio of 1.14 was obtained, while ratios of 1.13 and 1.2 were determined for the samples with $x=0.77$ and 0.82, respectively. In our case the lifting of the spin degeneracy can be explained by the fact that these QW structures are asymmetrically doped from both sides of the well ($N_{A2}>N_{A1}$), showing a higher carrier contribution coming from the lower doping layer.

The Shubnikov–de Haas oscillations were also measured at various temperatures between 0.3 and 10 K. The decrease of amplitude with increasing temperature can be used to determine the effective mass of the carriers.[15] In the studied systems the effective mass for each spin orientation of both $V_{3/2}$ subbands is different, due to the lifting of the spin degeneracy. In our measurements it was not possible to determine both effective masses separately, because the frequencies F_{SdH} of the oscillations, belonging to each particular spin orientation, are very close to each other. Nevertheless, since the difference in the carrier concentrations is relatively small, it can be assumed that the difference of the effective masses for the opposite spin orientations is also small. Therefore, an average heavy-hole mass $m^*_{3/2}$ was determined from the decrease of the SdH amplitude by increasing the temperature in the field range of $2\ T<B<6$ T. A parabolic subband dispersion was assumed. For the samples with $x=0.73$, 0.77, and 0.82 effective $m^*_{3/2}$ values of $(0.14\pm0.03)m_0$, $(0.12\pm0.03)m_0$, and $(0.14\pm0.03)m_0$ were calculated, respectively. Due to the spin splitting and the assumption of a parabolic subband the determined values are not very accurate. Especially for high hole densi-

ties, as reported here, strong deviations from the ideal parabolic behavior can be expected.[16]

If the obtained effective-mass values are compared with the heavy-hole mass of lattice-matched $In_{0.53}Ga_{0.47}As$ on InP ($m^*_{3/2}=0.42m_0$), a reduction of a factor of 3 due to the compressive strain was achieved. This fact is qualitatively in agreement with theoretical predictions of the $m^*_{3/2}$ values for biaxially strained bulk material as reported by Foulon *et al.*[17] A quantitative comparison with the calculated values of $m^*_{3/2}$ in Ref. 17 reveals a certain discrepancy, indicating that our measured values are systematically too large. This can be attributed to the quantization effect of the carriers in the QWs. The carrier confinement leads, in addition to the biaxial compressive strain, to a separation of the heavy- and light-hole subbands. Since the coupling of both subbands is altered, the effective mass is also modified. A further increase of the effective mass in a narrow QW can be due to the leakage of the hole wave function into the InP barrier layers. If the QW thickness is very small (for example, in sample 1989 with $d_{ch}=4$ nm), this effect can dominate resulting in a further improvement of the effective heavy-hole mass (see Table I).

B. Moderate- and high-field transport measurements

The transport characteristics of holes at moderate and high fields and also their dependence on vertical and longitudinal potentials were investigated using dc and magnetotransconductance (MT) measurements on 1 μm *p*-modulation-doped FETs (MODFETs), fabricated on the same samples. The devices had a gate width of $W=100$ μm. A high W/L_G ratio is necessary in order to improve the accuracy of the results if the geometric magnetoresistance measurement technique is employed.[18] Two types of MT measurements were performed: First, we kept V_{DS} constant and changed V_{GS} in order to obtain a mobility profile of the conducting channel. The method to determine the mobility μ at each bias point will be explained later. Second, we chose a particular V_{GS} value and measured a μ-V_{DS} profile at the given V_{GS}. From the measured μ values the average velocity v_{avg} of the carriers at the given bias conditions was calculated using the relation[19]

$$v_{avg}(E_{avg})=\mu(E_{avg})E_{avg}. \tag{2}$$

In order to estimate the average field E_{avg} under the gate of the studied MODFETs and its dependence of the applied voltages, we assumed the following simplifications: First, the applied gate-source voltage V_{GS} is responsible primarily for the position of the Fermi level in the QW, depleting (positive values) or enhancing (negative values) the whole hole concentration $p_S(V_{GS})$ in the channel; second, the applied drain-source voltage provides the confined carriers with kinetic energy, which is proportional to their velocity. Taking into account these considerations, we can calculate E_{avg} using the following equation:

$$E_{avg}(V_{DS},V_{GS})\approx k\frac{V_{DS}-2R_SI_D(V_{GS})}{L_G}=k\frac{V_{ch}}{L_G}, \tag{3}$$

where V_{DS} and V_{GS} are the applied voltages; I_D is the flowing drain current for the given bias point; $R_S\approx R_D$, the parasitic source resistance; and L_G is the gate length. Due to the inhomogeneous field distribution under the gate, an average factor k is necessary in order to get a more accurate value of the average field. For moderate V_{DS} values and a positive (depletion-mode) V_{GS} bias, the electric field $E(x)$ under the gate can be approximately described by a parabolic function,[20]

$$E(x)=\frac{E_{max}}{L_G^2}x^2\approx\frac{V_{ch}}{L_G^3}x^2. \tag{4}$$

If we define the average value of E_{avg} as the field where the channel voltage V_{ch} drops to 50% of its maximum, we can write

$$\int_0^{x_0}\frac{E_{max}}{L_G^2}x^2\,dx=\int_{x_0}^{L_G}\frac{E_{max}}{L_G^2}x^2\,dx, \tag{5}$$

and therefore

$$x_0=L_G\sqrt[3]{0.5}, \tag{6}$$

leading to

$$E_{avg}=E(x_0)=0.629E_{max}\approx0.629\frac{V_{ch}}{L_G}. \tag{7}$$

For the measurement range (-2 V$<V_{DS}<0$ V) the assumption of a parabolic field distribution between the source and drain ends of the gate (constant k factor: 0.629) was confirmed. Therefore, the calculated $v_{avg}(E_{avg})$ curves increase first with a nonlinear behavior and then saturate above a critical field, in accordance with theoretical calculations.[16] This indicates a dependence of μ on E of about E^{-1} in the saturation region, as is shown later.

First, we measured the dc transfer characteristics (I_{DS}-V_{GS}) of the devices and calculated the extrinsic transconductance ($g_{mext}\approx\partial I_{DS}/\partial V_{GS}$) profiles ($g_{mext}$-$V_{GS}$) of the same characteristics. At room temperature a quasisymmetrical g_{mext}-V_{GS} profile for the linear and saturation V_{DS} regimes was achieved in all samples.[7] Due to the enhanced thermal activation energy of the holes at 300 K ($k_BT=25$ meV) strong intersubband scattering and optical-phonon deformation potential scattering (nonpolar optical scattering) dominate in this temperature range.[21] For that reason both mobility and velocity values are strongly reduced (see Table I) and result in an averaged current transport between light and heavy holes. First at cryogenic conditions, where the optical phonon scattering becomes smaller [see Fig. 2(a)] and alloy and Coulomb scattering at ionized impurities[21] can play the dominant role, a strong dependence of the transfer curves (I_{DS}-V_{GS}, g_{mext}-V_{GS}) on V_{DS} was noticed. It must be pointed out that in our optimized structures Coulomb scattering can be neglected because of the relatively thick spacer layers ($\approx$10 nm). This fact can be observed in Fig. 2(a), where the mobility of the samples remains nearly constant for $T<40$ K.

In Figs. 5(a) and 5(b), typical dc transfer and transconductance characteristics, respectively, of one 1×100 μm^2 *p*-MODFET of the sample 1987 ($x=73\%$) at 77 K

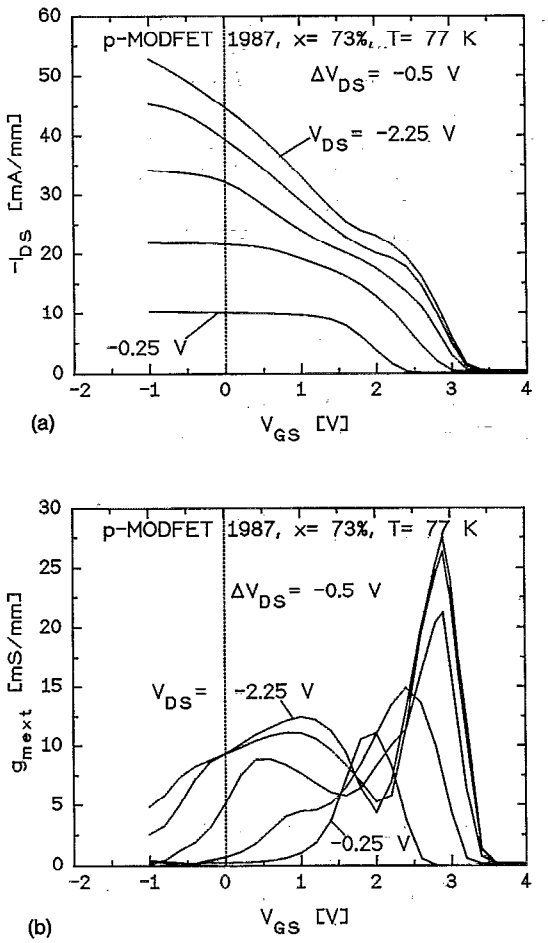

FIG. 5. (a) dc I_{DS}-V_{GS} and (b) g_{mext}-V_{GS} characteristics in dependence on V_{DS} of a 1×100 μm^2 $In_{0.73}Ga_{0.27}As/InP$ p-MODFET at 77 K. V_{DS} ranges between -0.25 and -2.25 V in -0.5 V steps.

are shown. V_{DS} was changed between -0.25 and -2.25 V in $\Delta V_{DS}=-0.5$ V steps. For this sample we measured a R_S value of 7 Ω mm (Ref. 7) at 77 K, using the end resistance method. Figure 5(a) shows for low-output voltages ($V_{DS}=-0.25$ V) only one V_{GS} interval where I_{DS} changes ($1.5\text{ V}<V_{GS}<2.5$ V). For higher V_{DS} (higher energies) a second interval ($-1\text{ V}<V_{GS}<1.5$ V) appears. This behavior can be better observed in Fig. 5(b), where the g_{mext}-V_{GS} profiles of the same measurement are plotted. Two effects take place if V_{DS} is increased. First, a second conducting channel appears at $V_{GS}\approx1$ V, indicating the increase of carrier population in a second subband. Second, the pinch-off voltage of the device changes, and the splitting of the g_m-V_{GS} curves in two current modulating regions becomes more pronounced. The first behavior can be explained as the excitation of part of the heavy holes from the $V_{3/2}$ subband into the $V_{1/2}$ subband, because of their improved energy, especially at the drain end of the gate. This effect is enhanced at higher fields, where a longer part of the channel reaches a critical field value E_0, enough to transfer carriers into the lower (higher in the case of electrons) subband. In our case, the QW design results in an energetic off-set between the light and heavy hole subbands, which is large enough to separate both types of carriers. This behavior can be observed especially at lower temperatures, where the thermal activation is low. The positive shift of the threshold voltage for higher V_{DS} values demonstrates the change of the Fermi-level position in the QW due to the enhancement of carrier population in the $V_{1/2}$ subband. Nearly the same behavior was observed in samples 1988 and 1989 because of their similar layer design compared with the sample 1987.

In order to better understand the dc experiments at 77 K, we measured the mobility μ distribution of the devices using the magnetotransconductance (MT) method. In the past this technique was employed on two-dimensional electron-gas (2DEG) systems by several groups[18,22] and is based on the geometric magnetoresistance effect. It is useful for the characterization of FETs, in which the parasitic series resistances have a negligible effect on the measured quantities,[18] which is the case of our structures at 77 K. By measuring the small-signal g_{mext} ($v_{gs}=0.1$ V, $f=1$ kHz) for a given V_{DS} as a function of V_{GS} with and without the presence of a magnetic field ($0.5\text{ T}\lesssim B\lesssim0.8$ T), a μ profile can be extracted from the relation[22]

$$\mu(V_{GS},V_{DS})=\frac{1}{B}\left(\frac{g_{mext}(V_{GS},V_{DS},B=0)}{g_{mext}(V_{GS},V_{DS},B)}-1\right)^{1/2}. \quad (8)$$

With our measurement setup only μ values in excess of 1000 cm^2/V s could be measured accurately because of the relatively low maximum magnetic field, which limits the measurement range in the case of low mobilities. For this reason we were able to measure only μ profiles at 77 K. The use of a small-signal voltage for the carrier modulation with a low amplitude ($v_{gs}=0.1$ V) compared with the dc V_{GS} operation range of the devices ($\Delta V_{GS}\approx2.5$–3.5 V) guarantees a good accuracy for the achieved local mobility μ at the given bias point (V_{DS},V_{GS}). The effect of the source resistance is eliminated in this measurement by taking the ratio of g_{mext} with and without magnetic field in Eq. (8). For the used small-signal measurement frequency ($f=1$ kHz) stationary conditions for the carrier distribution can be assumed. Figures 6(a) and 6(b) show the small-signal g_{mext}-V_{GS} and μ-V_{GS} profiles at 77 K, respectively, of a device from sample 1988 ($x=77\%$). For $V_{DS}=-0.2$ V only μ values in the range $1.2<V_{GS}<2.2$ V could be measured. For $V_{GS}<1.2$ V g_{mext} was too low to measure μ [see Fig. 6(a)] demonstrating the negligible population of the $V_{1/2}$ subband at low fields. First for $V_{DS}<-0.4$ V μ values corresponding to light holes could be measured. The μ curve for $V_{DS}=-1$ V in Fig. 6(b) shows two different mobility regions corresponding to both g_{mext} peaks (both subbands) of Fig. 6(a). The first region ranges from $0\text{ V}<V_{GS}<0.8$ V and shows μ values between 3060 and 3850 cm^2/V s, demonstrating that in this voltage region light-hole ($V_{1/2}$) transport dominates. The second region is the same as for $V_{DS}=-0.2$ V and shows lower μ values (between 2230 and 2920 cm^2/V s), which are attributed to the $V_{3/2}$ subband. Note that for this V_{DS} profile the maximum μ values for both regions are reached far away from the middle of the curve, where a minimum of 1960 cm^2/V s ($V_{GS}=1.2$ V) was measured. The reduction

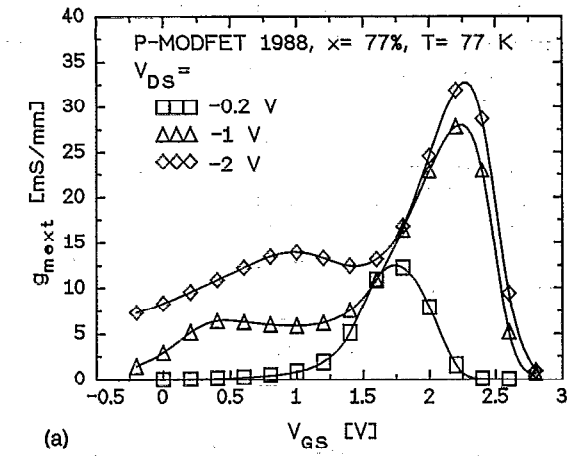

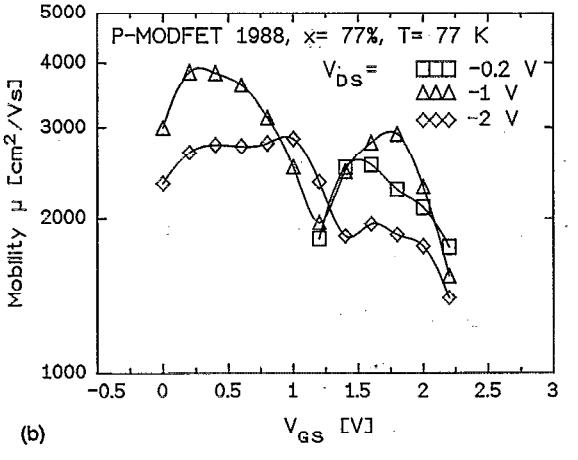

FIG. 6. (a) Extrinsic transconductance g_{mext}, and (b) mobility μ vs V_{GS} of a 1×100 μm^2 $In_{0.77}Ga_{0.23}As/InP$ p-MODFET for $V_{DS}=-0.2$ V (squares), -1 V (triangles), and -2 V (diamonds). Curves are extracted from magnetotransconductance measurements at 77 K using the following parameters: $v_{gs}=0.1$ V; $f=1$ kHz; $B=0.5$–0.8 T.

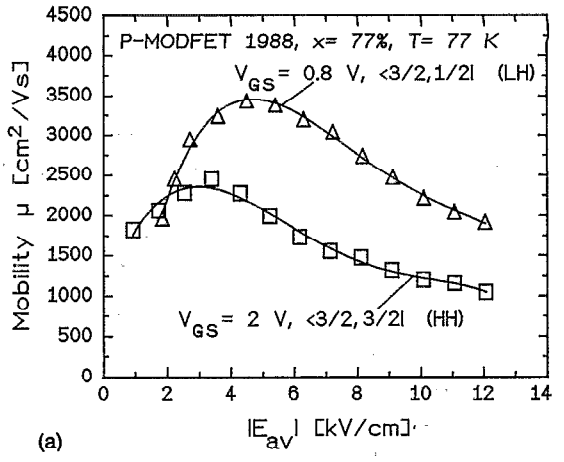

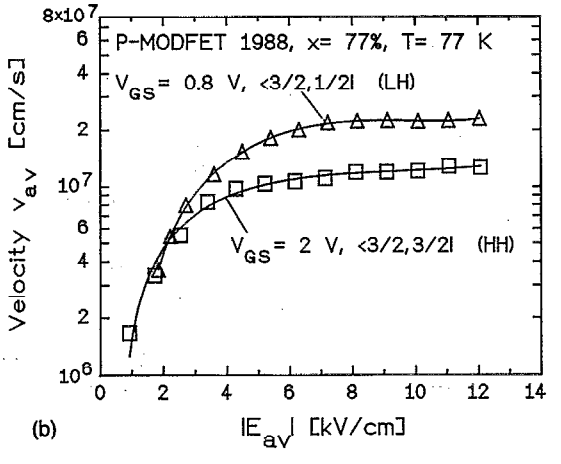

FIG. 7. (a) Mobility μ and (b) average velocity v_{avg} vs average electric field $|E_{avg}|$ at 77 K of the same device as in Fig. 6 for $V_{GS}=0.8$ V (light holes: LH) and 2 V (heavy holes: HH).

of the mobility in this voltage range is attributed to intersubband scattering. This fact indicates that at lower temperatures only a small amount of carriers suffer from this scattering mechanism compared with room temperature. Thus, one can say that at 77 K hole transport takes place in two energetically separated subband channels. Thermal activation results in a stronger interaction between both subbands and a consequent reduction of the average hole mobility. For the $V_{DS}=-1$ V curve in Fig. 6(b) mobility ratios of 1.96 and 1.49 were measured between the maximum values for the $V_{1/2}$ and $V_{3/2}$ and the minimum mobility at $V_{GS}=1.2$ V, respectively, indicating a reduction of 49% and 33% of the peak values for the HH and LH subbands, respectively. These results demonstrate that intersubband scattering has a strong effect on the transport behavior of this type of device. For $V_{DS}=-2$ V lower mobilities were measured in both subbands, indicating that other mechanisms become more important at higher fields.

In order to characterize the field dependence of μ and v_{avg} in both subbands at 77 K MT measurements were performed for $V_{DS}=0.8$ and 2 V, corresponding to LH and HH subbands, respectively. Figures 7(a) and 7(b) show the μ-E_{avg} and v_{avg}-E_{avg} plots, respectively, for $0<|E_{avg}|<12$ kV/cm ($0>V_{DS}>-2.5$ V). The E_{avg} values were calculated using Eq. (3), whereas the v_{avg} points result from Eq. (2).[19] In Fig. 7(a) a clearly distinct behavior for the mobility dependence on the field, compared with electrons on the same material,[23] can be observed. HH and LH reach their maximum μ values for fields of 3.5 and 4.4 kV/cm, respectively, and above this point mobilities decrease nearly linearly, indicating the enhancement of optical-phonon scattering at higher fields. This could explain the observation that the difference between the mobilities of both subbands decreases as the electric field increases,[23] as seen in Fig. 7(a). For low fields two reasons might be responsible for the reduction of μ: first, a strong intersubband scattering near the Γ point, which reduces both types of mobilities, and second, the E-$k_{\|}$ distribution of compressively strained 2DHG systems, which results in lower μ values for the LH subband ($\langle 3/2, 1/2|$) compared with the HH subband ($\langle 3/2, 3/2|$), in accordance with theoretical calculations.[3,4] This behavior can be clearly observed in Fig. 7(a), where both μ curves cross at a field of about 2 kV/cm. This field value may coincide with the $k_{\|}$ value, where the LH valence band crosses above the HH

valence band, causing the degeneracy of the zone-center region in the E-$k_{\|}$ distribution. This fact demonstrates that compressively strained p-type MODFETs, which normally work at higher fields (in the saturation I_{DS}-V_{DS} region), do not take advantage from this effect. Their enhanced transport properties originate more from other effects, such as the reduction of Coulomb scattering due to the modulation-doping concept or, in the case of lower temperatures, from the reduced intersubband scattering. Figure 7(b) shows the velocity-field characteristics of both subbands, calculated from Fig. 7(a). For fields higher than 7 kV/cm the v_{avg} saturates in both cases, but the saturation for the light holes is more pronounced. Saturation velocities of about $v_{avg}=1.2\times10^7$ and 2.2×10^7 cm/s were measured for HH and LH, respectively, at 77 K. These values are very high and underline the exceptionally good transport properties of 2DHG at low temperatures in the $In_xGa_{1-x}As/InP$ material system. At 300 K significantly lower saturation velocities, limited by the optical-phonon and intersubband scattering mechanisms, can be expected. If we compare the Hall mobilities at both temperatures [see Fig. 2(a)], we can easily see that $\mu_{77\ K}$ is about 10 times higher than $\mu_{300\ K}$. In the case of 2DEG on the same material system showing similar carrier concentrations a smaller difference between both mobility values ($\mu_{77\ K}/\mu_{300\ K}\approx5$) has been measured.[24] This fact demonstrates that in the case of holes a second mechanism, such as intersubband scattering, must be added to the optical-phonon scattering in order to explain the temperature dependence of the mobility.[16]

IV. CONCLUSION

The carrier transport at low, moderate, and high electric fields in MOVPE-grown single-quantum-well p-type modulation-doped $In_xGa_{1-x}As/InP$ ($0.73\leqslant x\leqslant0.82$) heterostructures has been investigated using several methods. Shubnikov–de Haas and quantum Hall-effect measurements at 50 mK revealed the existence of two-dimensional hole gases in all samples. Three populated subbands, two of them belonging to the highest heavy-hole state ($V_{3/2}$) and the third to the light-hole state ($V_{1/2}$), were detected in one of the samples ($x=73\%$). For higher indium contents ($x=77\%$, 82%) a reduction of the population of the $V_{1/2}$ subband was observed. This fact is attributed to the enhanced quantization due to the thinner QW thickness of these two samples. Spin splitting in the heavy-hole subbands originates from the lifting of the Kramers degeneracy due to the lack of inversion symmetry in the investigated QWs, resulting in population ratios for the split subbands of $1.13<p_{3/2,2}/p_{3/2,1}<1.2$. Using temperature-dependent SdH measurements effective heavy-hole masses in the range $0.12<m^*_{HH}/m_e<0.14$ were estimated. The measured values demonstrate the reduction of m^*_{HH} for compressive strained p-type 2DHG systems. For moderate and high fields and $T=77$ K a decoupling of current conduction in both subbands was observed with the help of dc measurements on MODFET devices, fabricated on the same samples. This behavior results from a lower intersubband scattering due to the reduced thermal activation of the carriers. This special effect, expected for highly populated 2DHG systems, was experimentally demonstrated for the first time. Mobility profiles (μ-V_{GS}) on all samples were also achieved at cryogenic conditions using the magnetotransconductance (MT) technique. A strong difference in the mobility μ of both subbands was measured. The μ-V_{GS} profiles showed a reduction of μ in the V_{GS} region where both types of holes interacted. Also with the help of the MT method, measurements of the velocity-field (v_{avg}-E_{avg}) characteristics for each subband were performed. A strong nonlinear behavior of μ vs E_{avg} for low fields was observed. At $E_{avg}\approx2$ kV/cm a crossover between the HH and LH μ-E_{avg} curves was measured. This effect was attributed to the crossing of both valence bands near the Γ point, in accordance with theoretical predictions for compressively strained 2DHG systems. The zone-center degeneracy of the E-$k_{\|}$ distribution does not have too much relevance for MODFET applications. It only enhances the low-field mobility and does not have any influence on the saturation velocity, which is limited by other scattering mechanisms. Intersubband scattering and optical-phonon scattering at 300 K and alloy scattering at 77 K were found as the limiting mechanisms for transport in the studied structures.

ACKNOWLEDGMENTS

We thank G. Nogueira Glenski and S. Böhme for technical assistance and G. Dietz and D. Leonhardt for the implementation of the magnetotransconductance and velocity-field measurement methods, respectively. Further, we are grateful to G. Müllejans for his assistance during the low-field magnetotransport measurements and also to Th. Klocke for helpful discussions.

[1] A. Mesquida Küsters, M. Stollenwerk, A. Kohl, M. Heuken, and K. Heime, in Proceedings of the 4th International Conference on InP and Related Materials, Newport, 1992, pp. 371–374.
[2] Y.-J. Chan and D. Pavlidis, IEEE Trans. Electron Devices **ED-39**, 466 (1992).
[3] M. Jaffe, Y. Sekiguchi, J. East, and J. Shing, Superlattices and Microstructures **4**, 395 (1988).
[4] M. Jaffe, Y. Sekiguchi, and J. Singh, Appl. Phys. Lett. **51**, 1943 (1987).
[5] M.-P. Houng and V.-C. Chang, J. Appl. Phys. **65**, 4990 (1989).
[6] T. Y. Wang and G. B. Stringfellow, J. Appl. Phys. **67**, 344 (1990).
[7] A. Mesquida Küsters, A. Kohl, V. Sommer, R. Müller, and K. Heime, IEEE Trans. Electron Devices **ED-40**, 2164 (1993).
[8] H. Temkin, D. G. Gershoni, S. N. G. Chu, J. M. Vandenberg, R. A. Hamm, and M. B. Panish, Appl. Phys. Lett. **51**, 1668 (1989).
[9] M. Glade, D. Grützmacher, R. Meyer, E. G. Woelk, and P. Balk, Appl. Phys. Lett. **54**, 2411 (1989).
[10] M. Glade, J. Hergeth, M. Stollenwerk, D. Grützmacher, and P. Balk, in Proceedings of the 17th International Symposium on GaAs, Jersey, 1990, pp. 579–584.
[11] F. J. Ohkawa and Y. Uemura, J. Phys. Soc. Jpn. **37**, 1324 (1974).
[12] H. L. Störmer, Z. Schlesinger, A. Chang, D. C. Tsui, A. C. Gossard, and W. Wiegmann, Phys. Rev. Lett. **51**, 126 (1983).
[13] M. Razeghi, P. Maurel, A. Tardella, L. Dmowski, D. Gauthier, and J. C. Portal, J. Appl. Phys. **60**, 2453 (1986).
[14] Y. Iye, E. E. Mendez, W. I. Wang, and L. Esaki, Phys. Rev. B **33**, 5854 (1986).
[15] G. A. B. Fowler, F. F. Fang, W. E. Howard, and P. J. Stiles, Phys. Rev. Lett. **16**, 901 (1966).
[16] E. P. O'Reilly, Semicond. Sci. Technol. **4**, 121 (1989).
[17] Y. Foulon, C. Priester, G. Allan, and M. Lannoo, in *Proceedings of the*

20th International Conference on the Physics of Semiconductors, Thessaloniki, Greece, edited by E. M. Anastassakis and J. D. Joannopoulos (World Scientific, Singapore, 1990), Vol. 2, p. 977.
[18] D. C. Look, G. B. Norris, W. Koop, T. Henderson, and H. Morkoç, Appl. Phys. Lett. **47**, 267 (1985).
[19] W. T. Masselink, W. Koop, T. Henderson, and H. Morkoç, IEEE Electron Device Lett. **EDL-6**, 539 (1985).
[20] Ch. A. Liechti, IEEE Trans. Microwave Theory Tech. **MTT-24**, 279 (1976).
[21] W. Walukiewicz, J. Appl. Phys. **59**, 3577 (1986).
[22] W. Prost, W. Brockerhoff, K. Heime, K. Ploog, W. Schlapp, G. Weimann, and H. Morkoç, IEEE Trans. Electron Devices **ED-33**, 646 (1986).
[23] W.-P. Hong, G. I. Ng, P. K. Bhattacharya, D. Pavlidis, S. Willing, and B. Das, J. Appl. Phys. **64**, 1945 (1988).
[24] A. Mesquida Küsters, Th. Funke, V. Sommer, R. Wüller, S. Brittner, A. Kohl, and K. Heime, Electron. Lett. **29**, 841 (1993).